Automatic Waveform Recognition from Complex RF Data with Filter-based Deep Learning

Bruce Hicks, Sabyasachi Biswas, Ajaya Dahal, Victor Gonzalez and Ali C. Gurbuz
Dept. of Electrical and Computer Engineering, Mississippi State University, MS, USA
{boh25, sb3682, ad2323, vg398}@msstate.edu, gurbuz@ece.msstate.edu

NAECON 2024 - IEEE National Aerospace and Electronics Conference | 979-8-3503-6762-1/24/$31.00 ©2024 IEEE | DOI: 10.1109/NAECON61878.2024.10670353

***Abstract*—Radar-based technologies have become ubiquitous in recent years, playing vital roles in many civilian and military applications, ranging from navigation to electronic warfare. With the widespread adoption of these technologies, several notable challenges have emerged, especially concerning spectrum congestion and the complicated interplay between radar and telecommunications signals. As such, accurate and fast recognition of radar waveforms is a necessity. Traditional techniques for waveform recognition, which often depend heavily on transforming raw RF data into alternative feature spaces such as time-frequency domain, have limitations due to low feature representation fidelity and high computational expense. To mitigate these issues, we propose a filter-based deep learning framework that learns directly from raw RF data. Unlike more conventional deep learning models, this framework includes parameterized filters with learnable cutoff frequencies. The inclusion of these filters enables the network to learn high-level features with clear physical interpretations. The initial validation of this model, including cases for both Sinc filters and Gabor filters, is done on a set of synthetic RF waveform receptions and achieves state-of-the-art performance with an overall accuracy of 97.4%, without any extensive data preprocessing.**

***Index Terms*—Radar waveform recognition, CVCNN, CV-SincNet, CV-GaborNet, RF sensing, learnable filter, micro-Doppler.**

I. Introduction

In modern society, radar-based technology has been integrated into numerous aspects of everyday life, ranging from various applications like human activity recognition (HAR) [1]–[5], defense and security [6]–[8], aviation and maritime navigation [9], mini-UAV classification [10], advanced driver assistance systems (ADAS) [11]–[13], indoor monitoring [14], [15], health monitoring [16], [17] and weather monitoring [18]. However, this proliferation has led to several noteworthy challenges, including the congestion of spectrum environments where radar systems must compete for access in a disorganized tangle of spectrum uses, especially against telecommunications [19]. This situation is even further complicated by the consideration of military-centric radar applications, such as threat detection, radar identification, jamming response, and other electronic warfare applications [20]. To assist in navigating this issue and developing strategic responses, waveform recognition in the RF spectrum has been given significant attention in research communities. The RF spectrum is a challenging environment consisting of various radar and telecommunication waveforms. Detecting and understanding the features of these waveforms across both time and frequency domains is critical, especially with the emergence of software-defined RF waveforms and 5G/6G telecommunications [21].

Current techniques for RF waveform recognition are often like those utilized in modulation recognition, as summarized in [22], [23]. These approaches primarily involve the transformation of raw complex RF data into some processed feature space, where engineered features may be extracted and prepared for the application of pattern recognition or machine learning techniques. A common feature space selected is some time-frequency domain representation, often in image format. This type of transformation may be explored more completely in related works such as [24]–[26]. However, these approaches face significant limitations due to the low fidelity of feature representation, which may often fail to capture the diverse and complex characteristics of RF waveforms fully. Also, the transformation of raw data into different domains can incur high computational costs, making these types of techniques ill-suited for real-time or close-to-real-time applications. Thus, it is desirable to instead develop techniques that can learn optimal features from complex raw data directly.

The emergence of deep learning frameworks, such as convolutional neural networks (CNN), provides the capability to learn directly from raw data. Several recent works [27]–[29] have leveraged this capability to great effect in waveform recognition. However, the performance and interpretability of such approaches remain refinable at this task. As such, we propose the application of a novel filter-based deep learning framework on raw complex RF data. Fundamentally, this approach is like the work done in [30], which utilizes a similar approach to perform radar-based human activity recognition. As such, the proposed approach is characterized by the inclusion of parameterized filters, which are intended to act as band-pass filters with learnable cutoff frequencies. This design allows the networks to learn high-level features with clear physical interpretations, boosting both the performance and interpretability of the model. To validate the proposed approach, a simulated RF data environment has been used to create an initial dataset and the performance of the model with Sinc and Gabor filters has been evaluated.

The presented work was funded in part by AFRL under ML-RCP program award # SPC-1000011554-GR131315 and the National Science Foundation (NSF) Award #2047771.

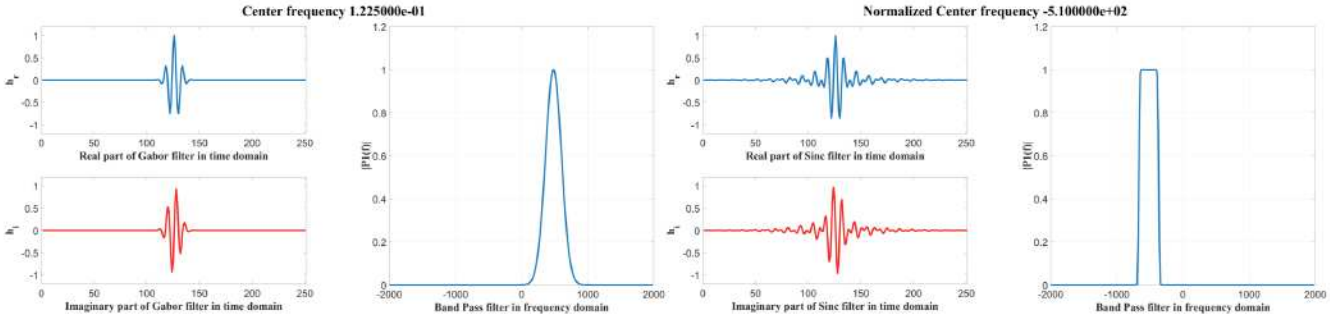

Fig. 1: Example of Sinc and Gabor filter in time and frequency domain

II. Proposed Methodology

In this section, we describe the formulation of real and complex-valued learnable filters designed to handle complex-valued input signal. To accommodate this, we incorporate structural changes in the filter definitions. These filters are characterized by two key learnable parameters: the center frequency f_c and the bandwidth B.

A. Complex Sinc filter banks

The Sinc layer involves learning a complex filter-bank, which consists of single-sided rectangular band-pass filters. The time-domain formulation of the complex Sinc filter is expressed as:

$$h_s[n, B, f_c] = 2BSinc(2\pi Bn) \times e^{j2\pi f_c n} \tag{1}$$

The designed filter is differentiable concerning its learnable parameters: the center frequency f_c and the bandwidth B, making it compatible with backpropagation. Each complex-valued Sinc filter is structured with equally-sized real and imaginary components, denoted as $h_s = h_{sr} + jh_{si}$.

$$h_{sr} = 2BSinc(2\pi Bn) \times cos(2\pi f_c n) \tag{2}$$

$$h_{si} = 2BSinc(2\pi Bn) \times sin(2\pi f_c n) \tag{3}$$

B. Complex Gabor filter banks

The impulse response of Gabor is defined by a sinusoidal wave multiplied by a Gaussian function. The time-domain formulation of complex Gabor filter is expressed as:

$$h_g[n, \sigma, f_c] = \sqrt{\frac{2}{\sqrt{\pi}\sigma}} e^{-\frac{n^2}{2\sigma^2}} \times e^{j2\pi f_c n} \tag{4}$$

where the σ is the variance. The relationship between sigma and -3dB bandwidth is given as follows,

$$\sigma = \frac{\sqrt{log(2)}}{\pi \times B} \tag{5}$$

so, the final equation of the complex Gabor filter having f_c and B as learnable parameter is,

$$h_g[n, B, f_c] = \sqrt{\frac{2\sqrt{\pi} \times B}{\sqrt{log(2)}}} e^{-\frac{n^2}{2\sigma^2}} \times e^{j2\pi f_c n} \tag{6}$$

Each complex-valued Gabor filter is structured with equally-sized real and imaginary components, denoted as $h_g = h_{gr} + jh_{gi}$.

$$h_{gr} = \sqrt{\frac{2}{\sqrt{\pi}\sigma}} e^{-\frac{n^2}{2\sigma^2}} \times cos(2\pi f_c n) \tag{7}$$

$$h_{gi} = \sqrt{\frac{2}{\sqrt{\pi}\sigma}} e^{-\frac{n^2}{2\sigma^2}} \times sin(2\pi f_c n) \tag{8}$$

The derivation of the Sinc filter h_s and Gabor filter h_g can be observed from Equation (1) and (6) respectively. An example of the Sinc and Gabor filter is shown in Fig. 1. Where -3dB bandwidth for the Gabor is 400 Hz and bandwidth of the Sinc is 300 Hz. The center frequency of the Gabor and Sinc are 490 and 510 Hz respectively. Equation (7) and (2) present the formulations of the real-valued versions of Gabor and Sinc filters respectively. The filters have a fixed window length $L = 125$ and the only learnable parameters are bandwidth B and center frequency f_c. For complex-valued operations f_c is initialized in the complete frequency range [-f_s/2,f_s/2], where f_s is the sampling frequency. For real-valued case f_c is initialized in the range $[0, f_s/2]$. In Fig. 2 the parametric filter block is shown.

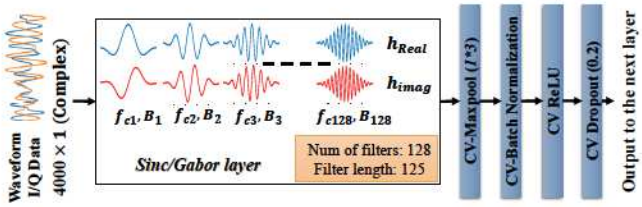

Fig. 2: The CV-Sinc/CV-Gabor Block

C. Complex Neural Network Layer Definitions

Complex neural network layers are adapted to complex algebra using real-number representations for complex values, with theoretical foundations supported by various studies [31]. A complex-valued tensor with N channels is represented by $2N$ channels: the first N for real parts and the next N for imaginary parts. Operations like convolution, activation, and pooling are adapted accordingly.

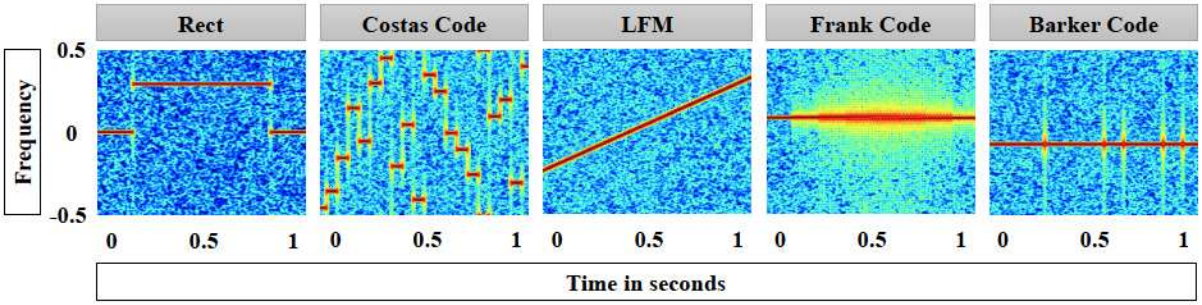

Fig. 3: Spectrogram result of different types of waveform.

1) Complex Fully Connected Layer: This layer uses complex algebra with real-number representations. For M neurons, it employs a complex weight matrix $W \in \mathbb{C}^{N\times M}$ and a complex bias vector $\beta \in \mathbb{C}^M$. Given a complex input $x \in \mathbb{C}^N$, the operation is:

$$Wx+\beta = \begin{bmatrix} \Re(W) & -\Im(W) \\ \Im(W) & \Re(W) \end{bmatrix} \begin{bmatrix} \Re(x) \\ \Im(x) \end{bmatrix} + \begin{bmatrix} \Re(\beta) \\ \Im(\beta) \end{bmatrix} \quad (9)$$

2) Complex Convolution Layer: Complex convolution uses real-valued representations for complex inputs and kernel weights. For a complex kernel matrix $W = W_R + jW_I$ and input $x = x_R + jx_I$, the operation is:

$$W * x = (W_R * x_R - W_I * x_I) + j(W_R * x_I + W_I * x_R) \quad (10)$$

3) Complex Activations: The complex ReLU function, $\mathbb{C}$ReLU, applies the ReLU function separately to the real and imaginary parts of a complex input x:

$$\mathbb{C}\text{ReLU}(x) = \begin{bmatrix} \text{ReLU}(\Re(x)) \\ \text{ReLU}(\Im(x)) \end{bmatrix} \quad (11)$$

The complex SoftMax function applies the standard SoftMax to the magnitudes of the complex output elements.

4) Complex MaxPooling Layer: This layer pools the complex value with the maximum magnitude to the next layer.

5) Complex Batch and Layer Normalization: Complex batch normalization shifts the mean to zero and scales by the inverse square root of the covariance matrix of the real and imaginary parts, using learnable parameters β (shift) and γ (scaling matrix):

$$\tilde{x} = \gamma x + \beta \quad (12)$$

III. Dataset Generation

To facilitate the evaluation of the proposed methodology, it is necessary to obtain a collection of received raw RF data with a known waveform shape upon transmission. For the initial validation of applying this type of methodology to this task, we elect to utilize purely simulated data; that is, we develop a reasonably-sized dataset of synthetic noisy waveform receptions.

A. Waveform Selection

The generated dataset consists of five common waveform modulations: linear frequency modulation (LFM), rectangular, Costas code, Barker code (binary phase code), Frank code (polyphase code). The example of each waveform is shown in Fig. 3. In this initial work, we include 500 samples of each of these modulations for a total of 2500 waveforms with corresponding ground truth labels. Each of these waveform types has several variables that are randomly varied to generate 2500 distinct waveforms to ensure the breadth of the dataset. Table 1 offers a full accounting of the parameters available for modulation, as well as the extent of their variation. This table also includes the range of added noise, which will be explained in the next section.

TABLE I: Parameter ranges for different types of waveform

Types	Parameters	Range of Values
ALL	f_c (center freq.)	$U\left[-\frac{f_c}{3}, \frac{f_c}{3}\right]$
	A (Amplitude)	$U[1, 10]$
	f_s (sampling freq.)	4000 Hz
	SNR	$U[0, 20]$
LFM	B (Bandwidth)	$U\left[\frac{f_c}{10}, f_c\right]$
Costas	f_{step} (num of freq steps)	$U[5, 20]$
	step_size	f_{step}/f_s
Barker	L_B (barker code length)	$\{7, 11, 13\}$
Frank	M (phase_steps)	$\{6, 7, 8\}$

B. Noise Addition

To simulate the physical transmission and reception process, a level of noise is added to the generated synthetic waveform receptions. This is done through a random dispersal of Gaussian noise across the RF data for each waveform. The magnitude of the added noise is determined by a randomly selected signal-to-noise (SNR) ratio value between 0 and 20 dB, as shown in the parameters listing in Table I.

IV. Performance Analysis of the Proposed Method

This paper compares the proposed approach with both a 2D CNN and a 1D CNN. The 2D CNN processes real 2D spectrogram images, whereas the 1D CNN, in both its real and complex versions, operates on 1D complex raw data. The

dataset is divided into 80% for training and 20% for testing across all architectures.

A. CNN2D architecture

The 2D CNN processes 128x128 μ-D spectrograms in grayscale. It consists of three convolutional layers (32, 32, and 64 filters, 3×3 kernel), each followed by max-pooling (3×3), batch normalization, ReLU activation, and 0.3 dropout. After flattening, it connects to a dense layer of size 128 with 0.5 dropout, leading to a softmax classifier outputting 5 classes.

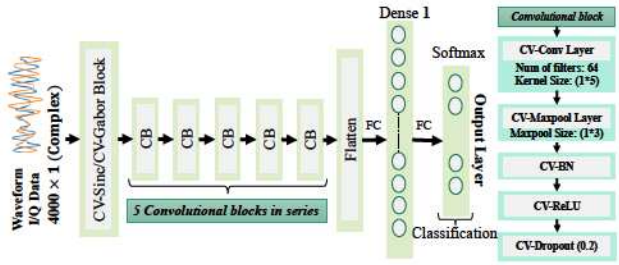

Fig. 4: Flow diagram of the Complex-valued SincNet/GaborNet architecture

B. 1D DCNN and Learnable Filter Based architectures

Six networks were implemented and tested on 1D raw data: CNN1D, SincNet (real), GaborNet (real), CV-CNN1D, CV-SincNet, and CV-GaborNet. These networks use input shapes of 4000×2, representing real and imaginary values. The Sinc and Gabor blocks in SincNet and GaborNet, respectively, contain 128 filters of 125 points each, followed by a max-pooling layer of size 1×5, normalization, ReLU activation, and 0.2 dropout. CV-CNN1D, CV-SincNet, and CV-GaborNet employ complex-valued computations in every layer. The main difference between CV-CNN1D and the learnable filter-based CNNs (CV-SincNet and CV-GaborNet) is that CV-CNN1D uses a standard CNN layer as the first layer instead of a Sinc/Gabor block. After the initial Sinc/Gabor block, the model consists of five convolutional blocks, a flattening layer, a dense layer of size 128, 0.3 dropout, and a softmax classifier. The architecture of the complex-valued learnable filter-based CNN is illustrated in Fig. 4.

C. Comparison Results

Table II presents the classification performance results for various architectures. CV-SincNet and CV-GaborNet achieve testing accuracies of 96.42% and 97.47%, respectively, outperforming CNN2D (RGB) by approximately 2.4% and 3.35%. These models also demonstrate superior precision, recall, and F1 scores compared to other models. SincNet and GaborNet achieve testing accuracies of 90.74% and 90.39%, respectively, which are about 8.68% and 10.08% lower than their complex-valued counterparts, underscoring the significance of complex-valued CNN networks. The relatively poor performance of CNN1D and CV-CNN1D highlights the effectiveness of using learnable filter-based networks as initial layers in neural network models.

TABLE II: Performance Comparison

Network	Testing Accuracy	Precision	Recall	F1 Score
CNN2D	94.02	96.6	94.07	93.95
CNN1D	62.84	72.76	61.68	62.57
SincNet	87.74	88.29	88.37	87.39
GaborNet	87.39	88.47	88.44	87.26
CV-CNN1D	63.48	74.09	63.57	63.23
CV-SincNet	96.42	97.87	95.25	96.34
CV-GaborNet	97.47	98.24	95.98	97.54

V. Conclusion and Future Work

In this work, we have explored the novel application of a filter-based deep learning model on waveform recognition and demonstrated its effectiveness in performing waveform recognition on raw complex RF data without any significant preprocessing. The proposed model achieved an overall accuracy of more than 96% and 97% on the synthetic dataset initially created for validation, using Sinc and Gabor filters respectively.

To fully establish the potential of this line of investigation, the simulated RF dataset must be extended to include a fuller sampling of common waveform types and a larger variety of noise additives. Additionally, work is being done to develop a software-defined radio-based hardware-in-the-loop procedure to generate pseudo-realistic waveform receptions in the laboratory environment. With this, the approach can be evaluated more thoroughly, including investigations of time costs and computational efficiency in real-time scenarios. Based upon these evaluations, a number of possible avenues of exploration are evident, such the type of filter to be included in the model.

Acknowledgments

This work was performed at the Information and Signal Processing Laboratory (IMPRESS) of the Electrical and Computer Engineering Department of Mississippi State University with funding provided by the Air Force Research Laboratory (AFRL) under awards # SPC-1000011554-GR131315.

References

[1] E. Kurtoğlu, S. Biswas, A. C. Gurbuz, and S. Z. Gurbuz, "Boosting multi-target recognition performance with multi-input multi-output radar-based angular subspace projection and multi-view deep neural network," *IET Radar, Sonar & Navigation*, vol. 17, no. 7, pp. 1115–1128, 2023.

[2] B. Debnath, I. A. Ebu, S. Biswas, A. C. Gurbuz, and J. E. Ball, "Fmcw radar range profile and micro-doppler signature fusion for improved traffic signaling motion classification," in *Proc. 2024 IEEE Radar Conference (RadarConf24)*, 2024.

[3] S. Gurbuz, Ed., *Deep Neural Network Design for Radar Applications*. London: IET, 2020.

[4] S. Biswas, A. Manavi Alam, and A. C. Gurbuz, "Hrspecnet: A deep learning-based high-resolution radar micro-doppler signature reconstruction for improved har classification," *IEEE Transactions on Radar Systems*, vol. 2, pp. 484–497, 2024.

[5] S. Biswas, C. O. Ayna, S. Z. Gurbuz, and A. C. Gurbuz, "Complex sincnet for more interpretable radar based activity recognition," in *2023 IEEE Radar Conference (RadarConf23)*, 2023, pp. 1–6.

[6] F. Fioranelli, M. Ritchie, and H. Griffiths, "Classification of unarmed/armed personnel using the netrad multistatic radar for micro-doppler and singular value decomposition features," *IEEE Geoscience and Remote Sensing Letters*, vol. 12, no. 9, pp. 1933–1937, 2015.

[7] Z. Ni and B. Huang, "Gait-based person identification and intruder detection using mm-wave sensing in multi-person scenario," *IEEE Sensors Journal*, vol. 22, no. 10, pp. 9713–9723, 2022.

[8] S. Björklund, T. Johansson, and H. Petersson, "Target classification in perimeter protection with a micro-doppler radar," in *2016 17th International Radar Symposium (IRS)*, 2016, pp. 1–5.

[9] M. Kirscht, J. Mietzner, B. Bickert, A. Dallinger, J. Hippler, J. Meyer-Hilberg, R. Zahn, and J. Boukamp, "An airborne radar sensor for maritime and ground surveillance and reconnaissance—algorithmic issues and exemplary results," *IEEE Journal of Selected Topics in Applied Earth Observations and Remote Sensing*, vol. 9, no. 3, pp. 971–979, 2016.

[10] A. Huizing, M. Heiligers, B. Dekker, J. de Wit, L. Cifola, and R. Harmanny, "Deep learning for classification of mini-uavs using micro-doppler spectrograms in cognitive radar," *IEEE Aerospace and Electronic Systems Magazine*, vol. 34, no. 11, pp. 46–56, 2019.

[11] S. Biswas, J. E. Ball, and A. C. Gurbuz, "Radar-lidar fusion for classification of traffic signaling motion in automotive applications," in *2023 IEEE International Radar Conference (RADAR)*, 2023, pp. 1–5.

[12] J. Kim, D. S. Han, and B. Senouci, "Radar and vision sensor fusion for object detection in autonomous vehicle surroundings," in *2018 Tenth International Conference on Ubiquitous and Future Networks (ICUFN)*, 2018, pp. 76–78.

[13] S. Biswas, B. Bartlett, J. E. Ball, and A. C. Gurbuz, "Classification of traffic signaling motion in automotive applications using fmcw radar," in *2023 IEEE Radar Conference (RadarConf23)*, 2023, pp. 1–6.

[14] S. Z. Gurbuz and M. G. Amin, "Radar-based human-motion recognition with deep learning: Promising applications for indoor monitoring," *IEEE Signal Processing Magazine*, vol. 36, no. 4, pp. 16–28, 2019.

[15] A. Dahal, S. Biswas, and A. C. Gurbuz, "Comparison between wifi-csi and radar-based human activity recognition," in *Proc. 2024 IEEE Radar Conference (RadarConf24)*, 2024.

[16] M. G. Amin, Y. D. Zhang, F. Ahmad, and K. D. Ho, "Radar signal processing for elderly fall detection: The future for in-home monitoring," *IEEE Signal Processing Magazine*, vol. 33, no. 2, pp. 71–80, 2016.

[17] F. Fioranelli and J. L. Kernec, "Contactless radar sensing for health monitoring," in *Engineering and Technology for Healthcare*, 2021, pp. 29–59.

[18] M. T. Falconi and F. S. Marzano, "Weather radar data processing and atmospheric applications: An overview of tools for monitoring clouds and detecting wind shear," *IEEE Signal Processing Magazine*, vol. 36, no. 4, pp. 85–97, 2019.

[19] Q. J. O. Tan and R. A. Romero, "Air vehicle target recognition with jammer nulling adaptive waveforms in cognitive radar using high-fidelity rcs responses," in *2018 International Conference on Radar (RADAR)*, 2018, pp. 1–6.

[20] C. B. Barneto, S. D. Liyanaarachchi, M. Heino, T. Riihonen, and M. Valkama, "Full duplex radio/radar technology: The enabler for advanced joint communication and sensing," *IEEE Wireless Communications*, vol. 28, no. 1, pp. 82–88, 2021.

[21] A. Jagannath, J. Jagannath, and P. S. P. V. Kumar, "A comprehensive survey on radio frequency (rf) fingerprinting: Traditional approaches, deep learning, and open challenges," 2022.

[22] W. Xiao, Z. Luo, and Q. Hu, "A review of research on signal modulation recognition based on deep learning," *Electronics*, vol. 11, p. 2764, 09 2022.

[23] O. Dobre, A. Abdi, Y. Bar-Ness, and W. Su, "Survey of automatic modulation classification techniques: Classical approaches and new trends," *IET Communications*, vol. 1, no. 2, pp. 137–156, 2007.

[24] J. Lunden and V. Koivunen, "Automatic radar waveform recognition," *IEEE Journal of Selected Topics in Signal Processing*, vol. 1, no. 1, pp. 124–136, 2007.

[25] C. Wang, J. Wang, and X. Zhang, "Automatic radar waveform recognition based on time-frequency analysis and convolutional neural network," in *2017 IEEE International Conference on Acoustics, Speech and Signal Processing (ICASSP)*, 2017, pp. 2437–2441.

[26] Z. Zhou, G. Huang, H. Chen, and J. Gao, "Automatic radar waveform recognition based on deep convolutional denoising auto-encoders," *Circuits, Systems, and Signal Processing*, vol. 37, no. 9, pp. 4034–4048, Sep. 2018.

[27] T. Huynh-The, C.-H. Hua, Q.-V. Pham, and D.-S. Kim, "Mcnet: An efficient cnn architecture for robust automatic modulation classification," *IEEE Communications Letters*, vol. 24, no. 4, pp. 811–815, 2020.

[28] T. Huynh-The, C.-H. Hua, V.-S. Doan, Q.-V. Pham, and D.-S. Kim, "Accurate deep cnn-based waveform recognition for intelligent radar systems," *IEEE Communications Letters*, vol. 25, no. 9, pp. 2938–2942, 2021.

[29] M. Wharton, A. M. Pavy, and P. Schniter, "Deep neural networks for radar waveform classification," in *2021 55th Asilomar Conference on Signals, Systems, and Computers*, 2021, pp. 1623–1627.

[30] S. Biswas, C. O. Ayna, S. Z. Gurbuz, and A. C. Gurbuz, "Cv-sincnet: Learning complex sinc filters from raw radar data for computationally efficient human motion recognition," *IEEE Transactions on Radar Systems*, vol. 1, pp. 493–504, 2023.

[31] C. Trabelsi, O. Bilaniuk, D. Serdyuk, S. Subramanian, J. F. Santos, S. Mehri, N. Rostamzadeh, Y. Bengio, and C. J. Pal, "Deep complex networks," *CoRR*, vol. abs/1705.09792, 2017.